Available online at www.sciencedirect.com
ScienceDirect
Journal of Sound and Vibration 320 (2009) 559–575
JOURNAL OF SOUND AND VIBRATION
www.elsevier.com/locate/jsvi

A novel method for the measurement of mechanical mobility

Scott A. Sands[a], Peter Camilleri[b], Rebecca A. Breuer[a], Gregory K. Cambrell[c], Robin J. Alfredson[d], Elizabeth M. Skuza[a], Philip J. Berger[a], Malcolm H. Wilkinson[a,*]

[a]*Ritchie Centre for Baby Health Research, Monash Institute of Medical Research, Monash University, Clayton, Victoria 3168, Australia*
[b]*PulmoSonix Pty. Ltd., 336A Glenhuntly Road, Elsternwick, Victoria 3185, Australia*
[c]*Department of Electrical and Computer Systems Engineering, Faculty of Engineering, Monash University, Victoria 3800, Australia*
[d]*Department of Mechanical Engineering, Faculty of Engineering, Monash University, Victoria 3800, Australia*

Received 22 August 2007; received in revised form 25 July 2008; accepted 15 August 2008
Handling Editor: J. Lam
Available online 5 October 2008

Abstract

We describe a novel technique for direct measurement of the unloaded driving-point mechanical mobility of a structure. The method uses an electrically-excited inertial motor/actuator attached directly to the structure under test (SUT) to induce sinusoidal motion in the frequency range 7.5–750 Hz. Two accelerometers, one attached to the actuator frame and the other to the vibrating actuator mass, separately measure the induced motion of the SUT and the vibrating mass. We develop an expression for the driving-point mobility of the SUT using these two measurements and show analytically that any mass-loading effect of the actuator on the measured mobility can be removed mathematically so that the unloaded mobility of the SUT can be determined. In this study we validate the method using a cantilever as a mobility standard. Measured mobility, mode shape and resonant frequency of cantilevers with various lengths were consistent with theoretical predictions for an unloaded cantilever. We conclude that the method can be used to conveniently determine the mobility of a range of structures, without the limitations associated with some of the traditional methods of mobility measurement.

1. Introduction

Mechanical mobility defines the willingness of a structure to move in response to a forced disturbance. Formally, mobility $\mathbf{Y}(j\omega)$ is the phasor ratio of the velocity of vibration $\mathbf{v}(j\omega)$ at a point on a structure to the applied force of vibration $\mathbf{F}(j\omega)$ [1–4], and is given by

$$\mathbf{Y}(j\omega) = \frac{\mathbf{v}(j\omega)}{\mathbf{F}(j\omega)} (\mathrm{m\,s^{-1}\,N^{-1}}) \tag{1}$$

*Corresponding author at: Ritchie Centre for Baby Health Research, Monash Institute of Medical Research, Monash Medical Centre, Clayton 3168, Australia. Tel.: +61395945398; fax: +61395946811.
E-mail address: mal.wilkinson@med.monash.edu.au (M.H. Wilkinson).

0022-460X/$ - see front matter © 2008 Published by Elsevier Ltd.
doi:10.1016/j.jsv.2008.08.012

Nomenclature

a	acceleration ($m\,s^{-2}$)
b	cantilever width (m)
C	compliance ($m\,N^{-1}$)
E	complex modulus (Pa), $E'(1+j\eta)$
E'	Young's modulus (Pa)
f	frequency (Hz)
F	force (N)
G	Green's function
I	cantilever moment of inertia (m^4)
j	imaginary unit
L	cantilever length (m)
M	mass (kg)
R	mechanical resistance ($N\,s\,m^{-1}$)
T	cantilever thickness (m)
v	velocity ($m\,s^{-1}$)
x	distance along cantilever from clamped end (m)
Y	mechanical mobility ($m\,s^{-1}\,N^{-1}$)
η	loss factor
μ	cantilever mass per unit length ($kg\,m^{-1}$)
ξ	fractional distance along cantilever, x/L
ρ	cantilever density ($kg\,m^{-3}$)
ω	radian frequency ($rad\,s^{-1}$)

Subscripts

1	refers to magnet kinetics
2	refers to frame and SUT kinetics
SUT	structure under test
m	magnet
f	frame
s	suspension

Abbreviations

MMD	mobility measuring device
FFT	fast Fourier transform
FRF	frequency response function
RV	residual volume
SUT	structure under test
TLC	total lung capacity

The magnitude $|\mathbf{Y}(j\omega)|$ describes the amplitude of the velocity of vibration given a unit applied force of vibration while the argument $\angle\,\mathbf{Y}(j\omega)$ represents the phase lead of the vibrational response to the applied force.

Mechanical mobility and related frequency response functions, such as mechanical impedance, dynamic compliance (receptance), and accelerance, are typically used for predicting the dynamic response of structures to vibrational excitation, for determining the modal properties of a structure (resonant frequencies, damping ratios, mode shapes), and for improving mathematical model accuracy [4]. Such analysis has important uses: in determining the dynamic response of stand-alone [5–9] and interconnected structures [10–18]; in the control of vibrational power transmission through coupled structures and in vibration isolation [13–15,18–30]; in crack detection, damage identification and condition monitoring [31–35]; and in the measurement of the damping or complex modulus properties of materials [36]. In the medical field, the mobility concept has been valuable for the quantification of biodynamic properties of the human body, such as the body surface [37], teeth [38], fingertip [39,40], whole body [41], joint dynamics [42], neuromuscular control of the arm and hand [43,44], and analysis of the organ of corti within the cochlear [45]. Further applications for mechanical mobility were outlined in an earlier review [46].

A complete description of the dynamic characteristics of a structure can be obtained by measuring rectilinear force and translational motion along three perpendicular axes, as well as moments and rotational motion about these axes, giving rise to an overall mobility matrix of size $6N \times 6N$ at N locations of interest [4]. However, for most practical applications the entire mobility matrix is not required and often it is sufficient to measure driving-point mobility by applying force and measuring velocity at the same location. Techniques currently available to measure driving-point mobility include impulse excitation with the use of an impact hammer, and attached vibration excitation using a shaker motor.

Impulse excitation involves the application of a measured force impulse to the SUT using an impact hammer and the simultaneous measurement of response velocity of the SUT (e.g. via an attached accelerometer or laser vibrometer). This method owes its popularity to the ease of selection and relocation of the excitation point, and, importantly, results in minimal structural loading allowing observation of the unloaded structural characteristics [47,48]. However, in practice, this method provides inherently limited

frequency resolution and signal-to-noise performance and it is susceptible to nonlinear effects [47,49]. Additionally, impact quality and consistency can be difficult to achieve [47], and the action of delivering an impulse, where all the force energy is delivered in a short period of time, may be inappropriate for application to fragile structures.

The attached vibration exciter method [50] involves a shaker motor which is used to drive an impedance head containing force and velocity transducers attached directly to the structure-under-test via a coupling rod. The primary advantage of this method is that the frequency, amplitude and duration of the oscillation can be controlled independently which gives accurate results, with considerable signal-to-noise performance and frequency resolution across a broad range of frequencies, compared with impulse excitation. However, this method is limited by practical complications in selection and relocation of the excitation point owing to the requirement for a support structure or a highly compliant suspension for the shaker motor.

To overcome practical limitations of the impact hammer and attached vibration excitation methods, we developed a novel technique for the measurement of driving-point mobility. The method is essentially a variant of the attached vibration excitation method but uses an inertial actuator attached to the SUT to provide sinusoidal force excitation. In our method, strategically placed accelerometers are used to measure the motion of the SUT and of the vibrating mass of the actuator. We will refer to this novel configuration of actuator and accelerometers as a mobility measuring device (MMD). In this paper we describe the design and validation of this method using a cantilever as a mobility standard. Our approach was to compare values of cantilever mobility measured using the MMD with calculated theoretical values based on the known dimensional and material properties of the cantilever.

2. Design

2.1. Principle

The MMD employs an electrically-driven inertial actuator (CSA, SA-1) to deliver an oscillatory force stimulus to a point on the SUT. The oscillatory force elicits an oscillatory response velocity at that same point proportional to the driving-point mobility of the SUT (see Fig. 1). Accelerometers (PCB ICP, Miniature and Lightweight 352A24, $100\,\mathrm{mV\,g^{-1}}$) are strategically placed within the device to measure the oscillatory acceleration and hence velocities of both the actuator magnet $\mathbf{v}_1(\mathrm{j}\omega)$ and the actuator frame $\mathbf{v}_2(\mathrm{j}\omega)$. Velocities are derived from accelerations by integration in the frequency domain, expressly $\mathbf{v}(\mathrm{j}\omega) = \mathbf{a}(\mathrm{j}\omega)/(\mathrm{j}\omega)$. The unknown SUT mobility, given by the velocity of the contiguous frame and SUT surface $\mathbf{v}_2(\mathrm{j}\omega)$ per unit applied force, as defined by Eq. (1), was derived from the analysis of the mechanical analogue shown in Fig. 1(b) giving the MMD equation:

$$\mathbf{Y}_{\mathrm{SUT}}(\mathrm{j}\omega) = \frac{-1}{\mathrm{j}\omega(M_m(\mathbf{v}_1(\mathrm{j}\omega)/\mathbf{v}_2(\mathrm{j}\omega)) + M_f)}(\mathrm{m\,s^{-1}\,N^{-1}}) \tag{2}$$

where M_m is the magnet mass and M_f is the frame mass.

Note that no direct measurement of the applied force using a force transducer is necessary. A full derivation of the MMD equation is provided in Appendix A. The device patent has been granted in the US [51] and is pending in the UK [52].

An important underlying principle of the method is that the loading effect of the frame mass on the structure is linearly removed by a single calculation, shown by Eq. (2), allowing measurement of the unloaded characteristic mobility (see Appendix B).

2.2. Device characteristics

The physical properties are summarised in Table 1. Electro-mechanical properties were determined using Thiele-Small tests (CLIOwin, Audiomatica). A single device resonance at 204 Hz was observed within the frequency range of the MMD as a result of the interaction between the magnet mass and the suspension stiffness. Importantly, increased magnet velocity at this resonance does not affect the ratio of magnet and frame velocities and therefore the mobility calculated using the MMD equation, Eq. (2), is unaffected.

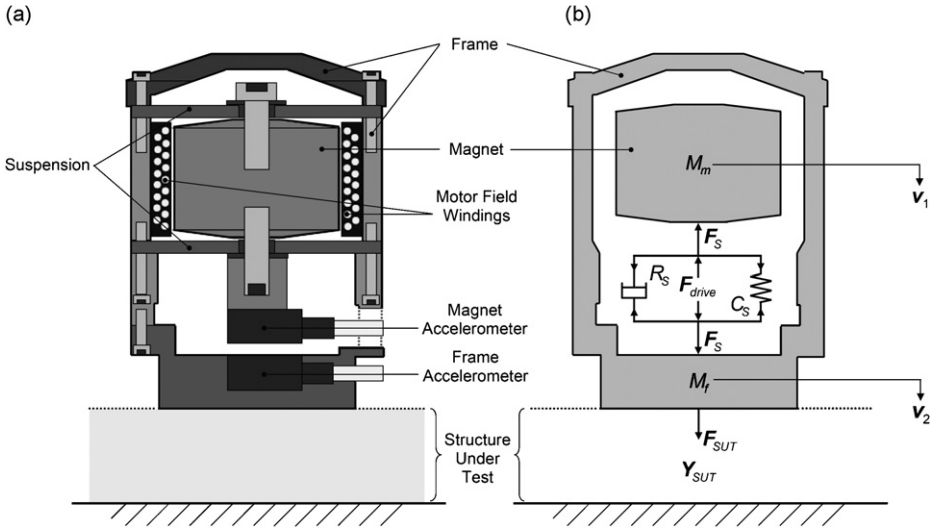

Fig. 1. (a) Schematic of the MMD showing the actuator frame coupled to a structure under test (SUT) for the measurement of its mobility. The internal permanent magnet interacts with the field produced by current through the field windings and transmits oscillatory force via the suspension to the frame/SUT. The oscillatory velocities of the magnet $\mathbf{v}_1$ and frame/SUT $\mathbf{v}_2$ are measured with the magnet and frame accelerometers, respectively. (b) Two degrees of freedom mechanical model of the MMD and coupled SUT shown as a lumped mobility. The forces represented by arrows are those of the suspension and drive acting upon the two masses, except $\mathbf{F}_{\mathrm{SUT}}$, which represents the applied force to the SUT. $\mathbf{F}_{\mathrm{drive}}$ represents the oscillatory driving force caused by the interaction of the electrical drive current through the motor field windings and the magnet as shown in (a). The mechanical resistance R_S and compliance C_S elements represent the suspension coupling the magnet to the frame that produces a force $\mathbf{F}_{R_s} + \mathbf{F}_{C_s}$ (arrows; not labelled) acting on the two masses to oppose the driving force, resulting in a net suspension force $\mathbf{F}_s$ developed between the magnet mass M_m and the frame mass M_f. The resultant applied force $\mathbf{F}_{\mathrm{SUT}}$ causes the applied surface of the SUT to move with a response velocity $\mathbf{v}_2$ proportional to its mobility $\mathbf{Y}_{\mathrm{SUT}}$.

Table 1
MMD properties

Parameter	Value
Dimensions	
Diameter	34.1 mm
Height	46.8 mm
Maximum allowable displacement (magnet-to-frame)	2.5 $\mathrm{mm}_{0-\mathrm{peak}}$
Physical masses	
Total	131.3 g
Frame mass, M_f	74.2 g
Magnet mass, M_m	44.6 g
Suspension mass	12.5 g
Exciter parameters (CSA SA-1), nominal	
Maximum force	1 $\mathrm{N}_{0-\mathrm{peak}}$
Bandwidth	20–1000 Hz
Maximum continuous current	1.0 $\mathrm{A}_{\mathrm{rms}}$
Electromechanical parameters:	
Resonant frequency, F_s	204 Hz
Mechanical mass, M_{ms}	47.3 g
Suspension stiffness, K_{ms}	77.5N mm^{-1}
Resistance, mechanical, R_{ms}	2.2 Ω_{M}
Magnetic field density × coil length, Bl	3.7 T m
Resistance, series electrical, R_e	5.8 Ω
Inductance, 1 kHz, L_e	0.78 mH

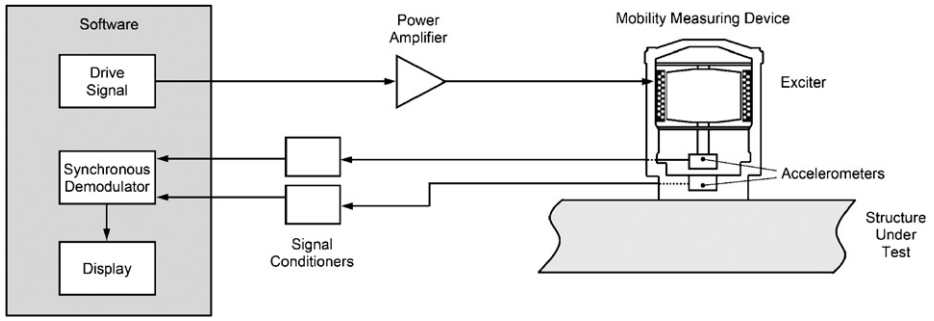

Fig. 2. Block diagram of the mobility measurement system.

The MMD was designed with a rigid external frame to avoid the potential for high-frequency frame bending modes which a non-rigid frame may engender, thus preventing differential effects on the frame and magnet velocities and hence mobility measurement.

The following sections detail the procedure used to verify the principle outlined in Section 2.1, including calibration of the mass terms in Eq. (2).

2.3. Mobility measuring configuration

The general setup for the measurement of the mobility of a SUT is illustrated in Fig. 2. The drive signal is output from software specifically developed for the control of the device (National Instruments LabVIEW Professional Development System Version 8.0, LabVIEW Sound and Vibration Toolset May 2003 Edition), via the data acquisition card (National Instruments, PCI-6052E 333kS/s, 16-Bit, 16-Analog-Input Multifunction DAQ) and the connector block (National Instruments Shielded Connector Block BNC-2110) and amplified (Sharp Optonica Stereo Amplifier SM-1515) in order to drive the inertial actuator. The magnet and frame accelerometers are connected to the data acquisition card via signal conditioners with gain factors of 1 and 10, respectively.

2.4. Software

The software module generates sinusoidal excitation discretely stepped in frequency for the actuator motor, synchronously demodulates the outputs from the accelerometers, and calculates the solution of Eq. (2) in real time. The module calculates a phasor representing the magnitude and phase of the magnet and frame accelerations for each discrete frequency of stimulation in the nominated frequency range. The excitation algorithm involves waiting a nominal *settling time* after commencement of each applied discrete frequency excitation to allow stabilisation for the mobility calculation. The frequency-dependent *settling time* function is defined by specification of a minimum time and minimum number of cycles so that there is a progressively longer settling time for lower frequencies. During the subsequent *integration time*, the acceleration signals for each given frequency are synchronously demodulated using the frequency of excitation to yield the magnitude and phase for each signal. The frequency-dependent *integration time* function is designed such that integration time rises linearly with the excitation period, minimising the overall computation time since the signal-to-noise ratio is greater at the higher frequencies. The drive amplitude is also tailored to counter the frequency-dependent behaviour of the actuator device itself, allowing for operation at low frequencies and in the vicinity of the actuator resonance at 204 Hz, and to maintain safe operation (with respect to rated current) and relatively constant amplitude of vibration with frequency, maximising the dynamic range. Continuous coherence analysis of the SUT accelerometer with respect to the excitation frequency is incorporated to ensure the quality of the SUT accelerometer signal.

The software settings used for the cantilever experiments were as follows: frequency range = 7.5–750 Hz; number of frequency increments = 1000; the settling time parameters were 0.15 s minimum and 40 cycle minimum; the integration time was 0.35 s at 750 Hz increasing to 25 s at 7.5 Hz (~200 cycles). Settings were

chosen experimentally such that the 95% confidence interval for mobility deduced by multiple measurements was within 3% of the mean on average across the frequency range.

3. Method

3.1. Determination of cantilever parameters for theoretical analysis

To determine the theoretical mobility of the cantilever, against which the MMD mobility measurements can be critically compared, the experimental determination of a range of cantilever parameters was required. A brass cantilever was chosen based on availability.

Dimensional parameters: Cantilever thickness T (3.24×10^{-3} m) and width b (50.65×10^{-3} m) were measured using digital callipers. Length L was measured using a steel metre ruler. The moment of inertia I (1.43×10^{-10} m^4) for a beam of rectangular cross-section was calculated from $I = bT^3/12$ [53]. The density ρ (8216.67 kg m^{-3}) was calculated from its weight and volumetric dimensions assuming uniformity; the value obtained was within the expected range for the material.

Complex modulus: The complex modulus of elasticity $\mathbf{E} = E'(1+j\eta)$ describes both the *Young's modulus* E' and the *loss factor* η, the latter representing losses due to internal friction. To determine $\mathbf{E}$, an impulse excitation experiment was performed to obtain an independent measure of the unloaded driving-point mobility of the cantilever, to which the theoretical cantilever mobility, calculated using Eq. (9), could be fit by adjusting $\mathbf{E}$ to match the mobility at first resonance.

For the impulse excitation measurement, an accelerometer was fixed at $x = L$ (Fig. 3). A precise impulse was delivered at the location of the accelerometer using the impact hammer (PCB ICP Impulse Force Test Hammer Model 086C03, sensitivity: 2.25 mV N^{-1}, impact tip: Super Soft Tip [Red] Model 084B11, frequency range [−10 dB]: 600 Hz). Appropriate signal conditioning, data acquisition (sampling rate 10 kHz), and signal processing (DC removal, raised cosine window) were utilised, according to ISO 7626-5 [47], to determine unloaded driving-point mobility.

Young's modulus: Young's modulus E' of the cantilever was determined experimentally using two independent methods. Firstly, E' was calculated using the measured unloaded fundamental resonant frequency f_1 of a cantilever of length 0.40 m based on the impulse excitation measurement (Fig. 4) and the equation for E' for a cantilever as re-arranged from Kinsler and Frey [54], given by

$$E' = f_1^2 \left[(1.194)^2 \frac{\pi}{8L^2} \frac{1}{\sqrt{\rho}} \frac{T}{\sqrt{12}} \right]^{-2} (\mathrm{N\,m^{-2}}) \tag{3}$$

Secondly, a static force deflection experiment was performed on a 0.40 m cantilever using masses of 100–1000 g in 100 g steps loaded at $x = 0.377$ m along the cantilever. The gradient of the linear force–displacement curve was calculated using a regression fit to yield the stiffness k of the cantilever for $x = 0.377$ m. E' was calculated using $E' = kx^3/(3I)$ N m^{-2} as rearranged from the equation for the stiffness of a long thin cantilever [53].

Loss factor: In contrast to the viscoelastic damping model ($\eta = \beta\omega$, β = constant) used by Scherer et al. [9], for our application we considered a hysteretic damping model which assumes that the loss factor η is independent of frequency, as commonly assumed for metal structures. The magnitude of η was determined by

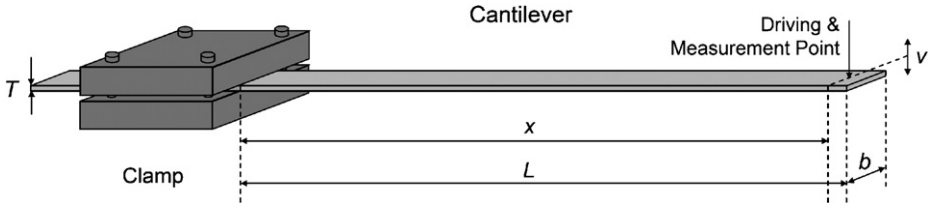

Fig. 3. Schematic of the clamped cantilever system. The driving and measurement point is located as close as possible to the end of the cantilever at distance x from the clamped end of the cantilever of length L. The measured oscillatory velocity $\mathbf{v}$ is perpendicular to the length L and width b of the cantilever. The thickness T of the cantilever is assumed to be uniform.

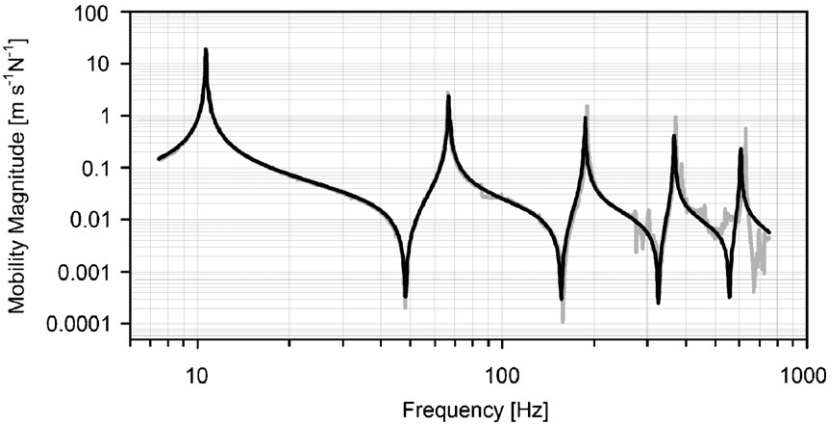

Fig. 4. Theoretical mobility magnitude compared with the impulse excitation measurement for the 0.40 m cantilever assuming hysteretic damping (——— theory; ——— impulse excitation). For the theoretical mobility, $E' = 87.3$ GPa was calculated based on the frequency of the first resonance (10.67 Hz) and $\eta = 5.6 \times 10^{-3}$ was adjusted to match the peak mobility of the first resonance. Note that the resonances have similar sharpness, demonstrating that the hysteretic damping model provided an accurate description of the damping of successive resonant and anti-resonant peaks. $\rho = 8216.67\,\mathrm{kg\,m^{-3}}$ and the dimensional parameters stated in Section 3.1 were used for the theoretical model.

adjusting η to achieve a good fit between the theoretical cantilever mobility and the measured mobility at the first resonant peak of the impulse excitation mobility measurement. Assessment of the validity of the viscoelastic damping model (over the measurement frequency range) was based on the quality of the fit between theory and measurement for resonant peaks 2–5.

3.2. Measurement of cantilever mobility

In order to both calibrate and validate the device, the driving-point mobility of the cantilever was measured using the MMD, for a range of cantilever lengths: 0.25–0.45 m in 0.05 m steps. The goal was to compare MMD measurements with theoretical predictions, specifically (1) mobility as a function of frequency for the 0.40 m cantilever, (2) the unloaded modal resonant frequencies for each length and (3) mobility at 8 Hz for each length. Calibration was performed based on (1) and validation based on (1)–(3).

The base of the MMD was attached to the upper side of the cantilever using a thin layer of thermoplastic hot-melt adhesive via a small-diameter light-weight circular washer. This arrangement placed the centre of mass of the MMD directly above the free end of the cantilever to approximate a point application at $x = L$ (see Fig. 3). Four bolts, equally and incrementally tightened to a torsion of 27.1 N m (20 ft lb) using a torsion wrench, provided effective and reproducible clamping of the cantilever. Stability of the clamp structure was aided by the application of an additional 20 kg mass to the base.

Resonant frequency vs cantilever length: To demonstrate the validity of the MMD measurements across the five cantilever lengths, the MMD values for the resonant frequencies f_n for the first four modes of vibration of the cantilever ($n = 1$–4) for each of the five cantilever lengths were compared with theoretical predictions from Kinsler and Frey [54]:

$$f_1 = (1.194)^2 \frac{\pi}{8L^2} \sqrt{\frac{E'}{\rho}} \frac{T}{\sqrt{12}} \text{ Hz} \tag{4}$$

$$f_2 = 6.267 f_1 \tag{5}$$

$$f_3 = 17.55 f_1 \tag{6}$$

$$f_4 = 34.39 f_1 \tag{7}$$

Notably Eqs. (4)–(7) are consistent with the cantilever theory described below. The MMD values were taken as the frequencies at which the phase of the mobility crossed zero.

3.3. Calibration

Masses of the magnet, frame and suspension were determined separately prior to the MMD assembly. The mass terms in Eq. (2) for the magnet M_m and frame M_f pre-calibration were based on the physical weights, and the (small) suspension mass was allocated to the magnet and frame terms in equal proportions. Because of the uncertainty of this allocation, using the 0.40 m cantilever length, we calibrated the proportion of suspension to be allocated to the mass and the frame terms M_m and M_f by adjusting each term to minimise the least squares difference, fine-tuning the MMD measurement to best fit the theoretical prediction near the first resonance. The calibrated values for M_m and M_f were used for all MMD measurements.

4. Cantilever mobility theory

In this section we present a simplified expression for the mobility of a long thin cantilever vibrating in air based on two recent studies [9,55].

4.1. General theory

Examination of an expression for the dynamic, small amplitude deflection $w(x,t)$ of a thin ($T \ll b \ll L$) isotropic cantilever of constant cross section, mass per unit length μ, subjected to a force per unit length $F(x,t)$ [55]:

$$\mathbf{E}I\frac{\partial^4 w(x,t)}{\partial x^4}+\mu\frac{\partial^2 w(x,t)}{\partial t^2}=F(x,t) \tag{8}$$

yields an equation for the mechanical impedance of the cantilever [9, their Eq. (27)]. The equation for the mobility of the cantilever described here was modified from the impedance form to

$$\mathbf{Y}(\mathrm{j}\omega)=\frac{\mathrm{j}\omega L^3\mathbf{G}(\xi,\xi,j\omega)}{\mathbf{E}I} \tag{9}$$

where time dependence is given by $e^{j\omega t}$ (as opposed to $e^{-j\omega t}$), and $\mathbf{G}(\xi, \xi, j\omega)$ is the Green's function, simplified from that of Scherer et al. [9, their Eq. (20)], as detailed in Appendix C.

5. Results

5.1. Determination of cantilever parameters for theoretical analysis

Young's modulus: $E' = 87.3 \pm 0.5$ GPa was determined experimentally using the measured unloaded resonant frequency $f_1 = 10.67 \pm 0.03$ Hz of the cantilever based on the impulse excitation measurement (Fig. 4). This measurement was verified using the force–displacement measurements as described in Section 3.1, giving $E' = 87.7$ GPa based on $k = 704.95\,\mathrm{N\,m^{-1}}$ at $x = 0.377$ m.

Loss factor: Adjustment of η to fit the magnitude of the first resonant peak in the theoretical model to the impulse excitation results yielded $\eta = 5.6 \times 10^{-3}$. Importantly, a good match of the magnitude of successive resonant and anti-resonant mobility peaks was observed between the theoretical and experimental impulse excitation results (Fig. 4), demonstrating that the hysteretic model was appropriate for use in the theoretical description for comparison with MMD measurements.

Adjustment of fractional length ξ: Experimentally, the fractional length ξ (x/L) approximated 1.0 by ensuring that the driving and measuring point x was as close as practicable to the free end of the cantilever, i.e. $x = L$. To best fit the location of the first anti-resonance from the impulse excitation experiment we adjusted x so that $x = L - 0.006$ m (6 mm from the free end of the cantilever). Such adjustment of ξ resulted in a left-shift of all of the anti-resonances but no other feature was affected i.e. resonant frequencies, damping and mode shape.

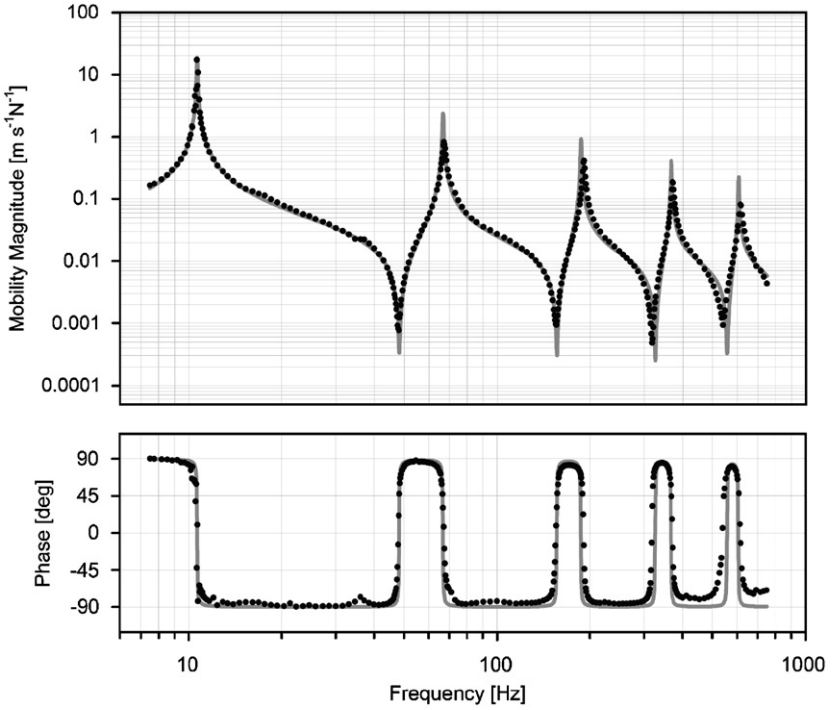

Fig. 5. Magnitude and phase of measured mobility (●) and theoretical mobility assuming hysteretic damping (———) plotted against frequency for the unloaded 0.40 m cantilever. Note the good agreement between measured and theoretical results across two decades of frequency (7.5–750 Hz) and 4.5 decades of magnitude from $<5\times10^{-4}$ to $>2\times10^{1}\,\mathrm{m\,s^{-1}\,N^{-1}}$.

5.2. Measurement of cantilever mobility

Mobility vs frequency: The results for mobility magnitude and phase as a function of frequency for the 0.40 m cantilever are plotted in Fig. 5 and compared with model predictions. The measured mobility result closely matched theory across two frequency decades (7.5–750 Hz). The mode shape (with respect to frequency) of the measurement was remarkably consistent with theory. Although not shown, the mode shapes for the measurement at other cantilever lengths were also consistent with theory. Note also the dynamic range of >4.5 decades achieved from $<5\times10^{-4}$ to $>2\times10^{1}\,\mathrm{m\,s^{-1}\,N^{-1}}$. The only disparity between the measurement and prediction (and impulse excitation experiment; Fig. 4) was the slight reduction in the observed sharpness of resonant peaks 2–5 (Fig. 5).

Resonant frequency vs cantilever length: Resonant frequency vs cantilever length for the first four modes of vibration is shown in Fig. 6 with the MMD data overlying the theoretical values based on Eqs. (4)–(7). Notably, the MMD measurements are consistent with the theoretical values for unloaded resonances.

Mobility vs cantilever length at 8 Hz: The measured mobility at 8 Hz as a function of cantilever length is shown in Fig. 7 plotted against the theoretical mobility calculated using Eq. (4) and a second theoretical mobility approximation based on $\mathbf{Y}(j\omega) = j\omega/k$, where k is the calculated static stiffness of the cantilever. Not surprisingly, all three curves asymptote together at cantilever lengths that are short compared to a wavelength, where inertial effects are small.

5.3. Calibration

Mass terms for the magnet M_m (physical mass 44.56 g) and frame M_f (physical mass 74.21 g) prior to calibration were the true physical masses with the addition of the allocation of half of the suspension mass (physical mass 12.50 g), therefore $M_m = 50.81$ g and $M_f = 80.46$ g. Note the total mass of the three components = 131.27 g. The results of the calibration yielded $M_m = 51.81$ g, $M_f = 79.56$ g. Note that the total

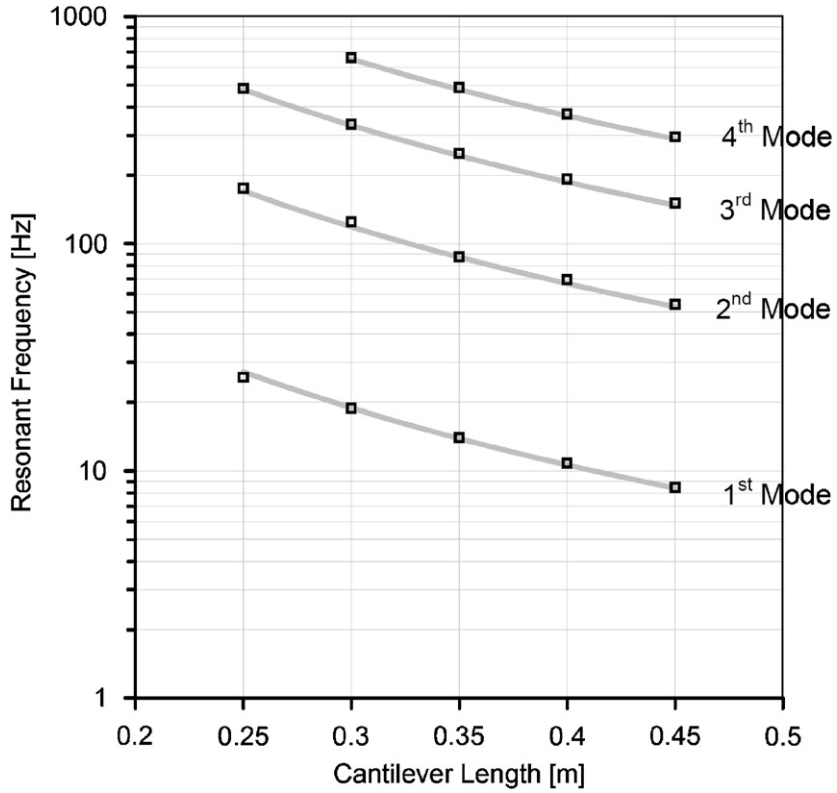

Fig. 6. Modal resonant frequencies for various cantilever lengths. Note that the measured unloaded resonance frequencies (□) are in good agreement with the theoretical predictions (———) for each of the cantilever lengths. The theoretical curves are based on Eqs. (4–7) [54], using $E' = 87.3\,\text{GPa}$, $\rho = 8216.67\,\text{kg m}^{-3}$, and $T = 3.24 \times 10^{-3}\,\text{m}$.

mass post-calibration = 131.37 g. Effectively, the suspension mass was allocated 58% to M_m and 42% to M_f with an additional increase in M_f by 0.1 g. It is important to note that the calibration minimally affected the mobility, i.e. pre-calibration the resonant frequency for the 0.40 m cantilever as measured by the MMD was 10.79 Hz whereas post-calibration the measurement was 10.63 Hz compared to the 10.67 ± 0.03 Hz from the impulse excitation results.

6. Discussion

We have demonstrated the validity of a novel method for the measurement of mechanical mobility. Our measurements of mobility as a function of frequency for the 0.40 m cantilever, and the unloaded modal resonant frequency for various cantilever lengths (Figs. 5–7), are in excellent agreement with theoretical predictions across a broad range of frequencies (2 decades) with impressive dynamic range (4.5 decades). The key finding of this study is that mechanical mobility can be measured accurately by the direct application of an inertial actuator to a SUT using appropriately placed accelerometers, despite the loading effect of the MMD.

6.1. Strengths and limitations

A major strength of the method is the inherent lack of sensitivity to magnet velocity around the single device resonance at 204 Hz, at which the magnet and suspension interact to produce a large magnet oscillation relative to the drive current. Notably the resonance does not interfere with the measurement of the mobility of the cantilever, as can be seen from Figs. 5, 6 and 8, where no artefacts can be observed at or near 204 Hz. Examination of the MMD equation, Eq. (2), reveals that the mobility is calculated as the ratio of the velocity

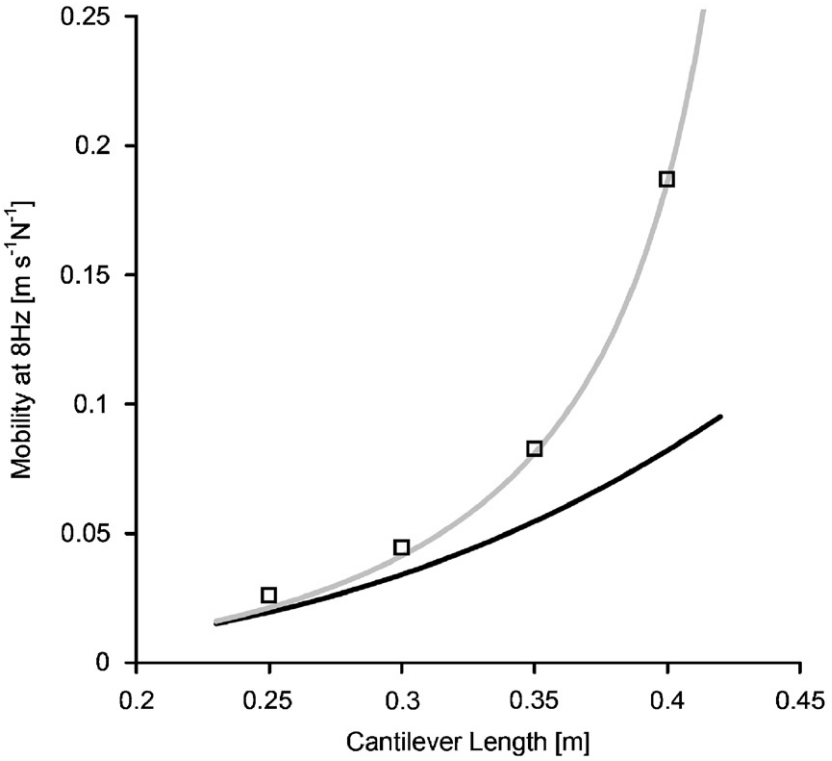

Fig. 7. MMD mobility measurements at 8 Hz vs theoretical model mobility and the mobility of a pure theoretical stiffness for various cantilever lengths (—— pure stiffness; —— theory; ▫ MMD). Note that the MMD mobility measurements at 8 Hz are in good agreement with the theoretical model. Also note the convergence of the MMD and theoretical model results with the pure theoretical stiffness ($k = 704.95\,\mathrm{N\,m^{-1}}$) at lower cantilever lengths where inertial effects are expected to become negligible and accordingly cantilever stiffness dominates the measured mobility.

of the magnet and frame, and not the magnet or frame velocity alone (which are not differentially affected by the resonance); thus changes in the amplitude of the magnet vibrations are accounted for in the calculation of mobility. Furthermore, the drive current can be tailored to limit the amplitude of oscillation within the constraint of maximum displacement and the potential for overdriven charge amplifiers. The dynamic characteristics of the device itself therefore do not influence the mobility measured using this method, within the frequency range examined.

Potential performance limitations of the MMD include those intrinsic to the inertial actuator: maximum force (1 N_{0-peak}), maximum continuous current (1 A_{rms}), and bandwidth (20–1000 Hz). Selection of an inertial actuator for an application must consider these limitations in terms of the force required to provide sufficient oscillations of the SUT for accurate measurement above the noise floor. Mobility measurement at low frequencies poses the greatest challenge; measurement is limited by not only signal-to-noise ratio, but the inherent reduced magnet velocity due to the drop off of delivered force by an inertial actuator below resonance. This effect can be minimised by lowering the resonant frequency through a reduction in the suspension stiffness. The drive amplitude is also limited by the maximum allowable displacement of the MMD (magnet relative to frame, 2.5 mm_{0-peak}) which requires consideration for operation near maximum force or maximum continuous current, also particularly relevant at low frequencies. However, in our application measurement of mobility was possible even below the lower limit of the bandwidth of the inertial actuator (20 Hz), to as low as 7.5 Hz, demonstrating that these limitations can be successfully overcome.

In the ideal scenario of linearity of the SUT, the effect of mass loading the system is accounted for by a linear subtraction of the mobility associated with the actuator mass (see Appendix B). By contrast, if the system were to be highly nonlinear, such that a large displacement shifts the system operating point to a

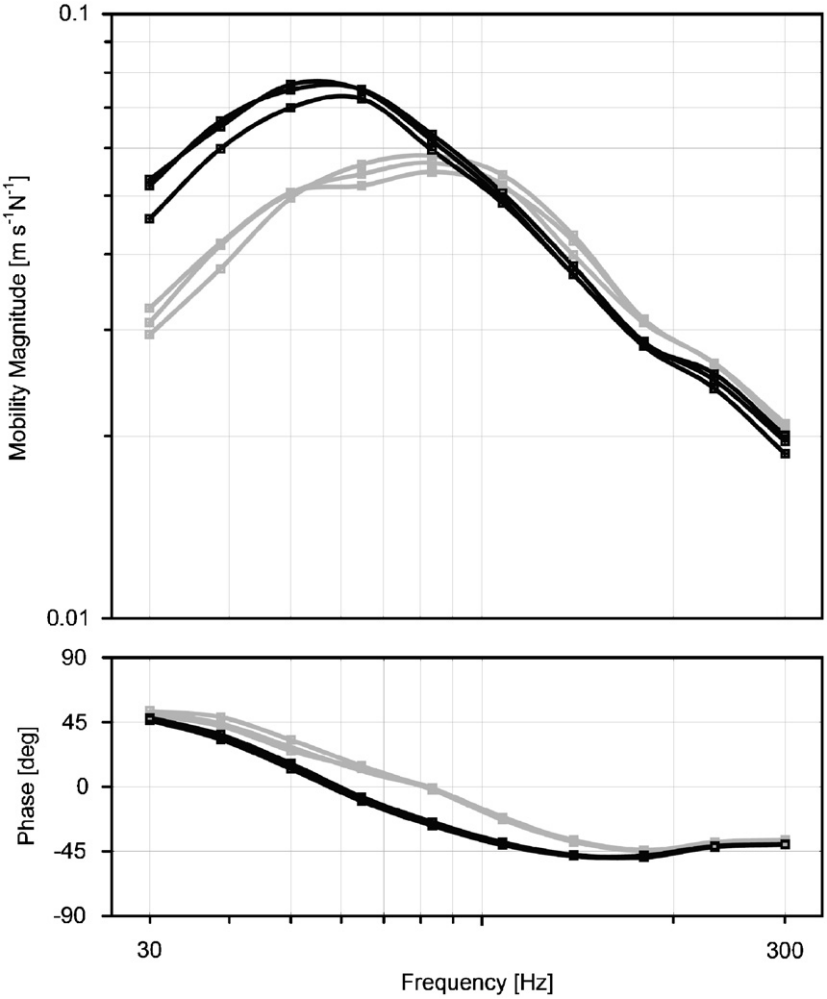

Fig. 8. Chest mobility magnitude and phase (residual volume (RV); total lung capacity (TLC)). Three chest mobility measurements were made at maximum lung volume (TLC) and minimum lung volume (RV) with a single male subject (85 kg) holding his breath for the duration of each measurement. A rigid and firmly attached thin coupling disc of 5 cm diameter was used to couple the MMD to the chest wall. Its potential effect on the measurement of chest mobility was removed by including its mass (28.30 g) in the frame mass of the MMD. Note that the chest wall closely resembles the mobility of a first-order mechanical resonant circuit with a stiffness k, mass M and a relatively high damping. Increasing the inflation of the lungs from RV to TLC increased stiffness k, as shown by the downwards vertical translation of the stiffness-dominated low-frequency region of the mobility curve where $\mathbf{Y}(j\omega) = j\omega/k$. Inspection of the mass-dominated high-frequency region of the mobility curve where $\mathbf{Y}(j\omega) = 1/(j\omega M)$ indicates that the chest wall mass was relatively stable during inflation. Consequently, the chest resonance at $f_0 = (k/M)^{0.5}/(2\pi)$ lies rightwards at a higher frequency (from ~55 to ~80 Hz).

substantially different (small-signal) mobility, the mass loading effect would not be adequately accounted for by linear subtraction. To address this theoretical possibility, we made several determinations of mobility at different actuator drive levels. The mobility determined at each frequency remained invariant with drive level. This finding strongly supports the assumption of linearity.

The MMD measurement shown in Fig. 5 suggests an increased measured damping (loss modulus) at higher frequencies or higher order modes from fundamental. Note the second resonant peak is lower in the MMD measurement than predicted by theory, perhaps reflecting suppression or increased damping as a result of second order effects; potential sources of damping are the somewhat rigid wire connecting the power amplifier to the inertial actuator for the supply of drive current or an aerodynamic damping effect of the vibrating MMD.

6.2. Applications

The MMD could be particularly useful where it is impractical to set up an attached vibration exciter requiring a mounting, where it is inappropriate to expose moving components, where applying an impulse from an impulse hammer may damage the structure, or for mobility measurements where the ability to operate the device in isolation is important. We envisage four potential applications in which the MMD may be practicable beyond those already mentioned in the introduction.

(1) Dynamic fluid viscosity could be measured by measuring the damping effect of the fluid on the vibration of the MMD. For this application, the MMD would be mounted on the end of a cantilever and submerged within a container holding the fluid. In this setting, we can predict explicitly the viscosity given the measured mobility of the cantilever using the analysis of Sader [55] and Scherer et al. [9].
(2) By using an additional accelerometer to measure the velocity at a remote location the transfer mobility could be measured using the force equation, Eqs. (16) and (1).
(3) In a passive form (without drive capabilities) the MMD may have the potential to measure mobility using the energy from spontaneous vibrations on or within a structure.
(4) The practicality of our method allows for potential use outside the field of engineering. Clinical examination of the chest of adult patients using manual percussion is commonly used to qualitatively establish the degree of inflation of the lungs and to identify other potentially serious clinical conditions such as pneumothorax (air entry to the intrapleural space). The MMD might be used to achieve a more quantitative measure of lung inflation or lung condition if a relationship could be established between chest mobility and lung inflation. To explore this possibility, a calibrated MMD was attached to a supine adult male's chest with a tape adhesive and it was used to measure chest mobility while the subject was asked to hold his breath first at full inspiration (total lung capacity or TLC) and then at full and forceful expiration (residual volume RV). The procedure was repeated three times. The mobility measurements (Fig. 8) show quite clearly that lung inflation influences chest wall mobility, demonstrating the practical utility of the MMD in a situation where application of mounting is impractical and impact testing is inappropriate.

6.3. Device improvements

Further work in MMD design may include tailoring of the drive signal based on the amplitude of vibration of the SUT to improve the signal-to-noise ratio at the SUT accelerometer output and to improve the dynamic range of the mobility measurement. A control loop could also be introduced to make SUT-signal-coherence-based alterations in integration time such that the integration moves to the next discrete frequency only after a pre-specified error criterion is reached. Likewise, an algorithm could be introduced to recognise when transients have fallen below a specified fraction so that settling time can be minimised. Such changes to the device would speed up operation without compromising accuracy.

A final improvement would be to generate the drive signals internally within the MMD itself and to use a radio link to telemeter measurement instructions to the MMD and to telemeter measured accelerometer data from the frame and actuator magnet back to a remote analyser. This would obviate the need for cables connecting the MMD to an external processor, thus removing any potential for mechanical damping of the MMD at high frequencies.

7. Conclusion

A novel mechanical mobility measurement method has been described theoretically and validated experimentally. Both the mobility measurement method and the calibration technique may find application in the quantitative measurement of mechanical mobility. Our demonstration that the impact of mass loading of the SUT can be removed, by mathematical means, enhances the practicality of the method for precisely measuring mobility in engineering and medical applications.

Acknowledgements

The financial support of the National Health and Medical Research Council of Australia, Development Grant Number 237045, and Premier Bionics Limited, is gratefully acknowledged. We gratefully acknowledge John E. Sader, Marc P. Scherer, and John Davy for useful discussions. We would also like to thank Bradley Edwards for his assistance with the chest mobility experiments.

Appendix A

A.1. Derivation of the MMD equation, Eq. (2)

The unknown mobility $\mathbf{Y}_{\mathrm{SUT}}(\mathrm{j}\omega)$ is defined by the velocity $\mathbf{v}_2(\mathrm{j}\omega)$ of the frame and SUT-surface per unit applied force $\mathbf{F}_{\mathrm{SUT}}(\mathrm{j}\omega)$:

$$\mathbf{Y}_{\mathrm{SUT}}(\mathrm{j}\omega) = \frac{\mathbf{v}_2(\mathrm{j}\omega)}{\mathbf{F}_{\mathrm{SUT}}(\mathrm{j}\omega)} \tag{10}$$

The forces acting to accelerate downwards the magnet and frame masses, shown in Fig. 1(b) are given by

$$\sum \mathbf{F}_1(\mathrm{j}\omega) = -\mathbf{F}_s(\mathrm{j}\omega) \tag{11}$$

$$\sum \mathbf{F}_2(\mathrm{j}\omega) = \mathbf{F}_s(\mathrm{j}\omega) - \mathbf{F}_{\mathrm{SUT}}(\mathrm{j}\omega) \tag{12}$$

The net suspension force is given by $\mathbf{F}_s(\mathrm{j}\omega) = \mathbf{F}_{\mathrm{drive}}(\mathrm{j}\omega) - \mathbf{F}_{R_s}(\mathrm{j}\omega) - \mathbf{F}_{C_s}(\mathrm{j}\omega)$ where the reaction forces are given by $\mathbf{F}_{R_s}(\mathrm{j}\omega) = R_s(\mathbf{v}_2 - \mathbf{v}_1)$ and $\mathbf{F}_{C_s}(\mathrm{j}\omega) = (\mathbf{v}_2 - \mathbf{v}_1)/(\mathrm{j}\omega C_S)$. Combining Eqs. (11) and (12) yields the cancellation of this force term and representation of $\mathbf{F}_{\mathrm{SUT}}(\mathrm{j}\omega)$ in terms of the net forces applied to the mass elements. Thus Eq. (13) states mathematically that the downwards force applied to the SUT surface is equal to the upwards net force accelerating the magnet mass less the downwards force required to accelerate the frame mass:

$$\mathbf{F}_{\mathrm{SUT}}(\mathrm{j}\omega) = -\sum \mathbf{F}_1(\mathrm{j}\omega) - \sum \mathbf{F}_2(\mathrm{j}\omega) \tag{13}$$

Representation of the sums of forces in terms of the masses and their accelerations and integrating to achieve velocity yields Eqs. (14) and (15) and combining with Eq. (13) yields Eq. (16):

$$\sum \mathbf{F}_1(\mathrm{j}\omega) = M_m \mathbf{a}_1(\mathrm{j}\omega) = \mathrm{j}\omega M_m \mathbf{v}_1(\mathrm{j}\omega) \tag{14}$$

$$\sum \mathbf{F}_2(\mathrm{j}\omega) = M_f \mathbf{a}_2(\mathrm{j}\omega) = \mathrm{j}\omega M_f \mathbf{v}_2(\mathrm{j}\omega) \tag{15}$$

$$\mathbf{F}_{\mathrm{SUT}}(\mathrm{j}\omega) = -\mathrm{j}\omega M_m \mathbf{v}_1(\omega) - \mathrm{j}\omega M_f \mathbf{v}_2(\mathrm{j}\omega) \tag{16}$$

Combining Eqs. (16) and (10) yields the MMD equation, as in Eq. (2):

$$\mathbf{Y}_{\mathrm{SUT}}(\mathrm{j}\omega) = \frac{-1}{\mathrm{j}\omega(M_m(\mathbf{v}_1(\mathrm{j}\omega)/\mathbf{v}_2(\mathrm{j}\omega)) + M_f)}$$

Appendix B

B.1. Derivation of the MMD equation, Eq. (2), in terms of loaded mobility and frame mass mobility

$\mathbf{Y}_{\mathrm{SUT}}(\mathrm{j}\omega)$ can be derived from the measured frame-mass-loaded mobility $\mathbf{Y}_{\mathrm{SUT,loaded}}(\mathrm{j}\omega)$ by performing a linear subtraction of the mobility of the frame mass $\mathbf{Y}_{M_f}(\mathrm{j}\omega) = 1/(\mathrm{j}\omega M_f)$ from $\mathbf{Y}_{\mathrm{SUT,loaded}}(\mathrm{j}\omega)$. The frame and SUT are represented as mobility elements in parallel since velocity $\mathbf{v}_2(\mathrm{j}\omega)$ is the common across variable, and therefore:

$$\mathbf{Y}_{\mathrm{SUT}}(\mathrm{j}\omega) = [\mathbf{Y}^{-1}_{\mathrm{SUT,loaded}}(\mathrm{j}\omega) - \mathbf{Y}^{-1}_{M_f}(\mathrm{j}\omega)]^{-1} \tag{17}$$

To complete the derivation, and demonstrate the consistency between Eq. (17) and the MMD equation, Eq. (2), an expression for the frame-mass-loaded mobility $\mathbf{Y}_{\mathrm{SUT,loaded}}(\mathrm{j}\omega)$ is required. The applied force $\mathbf{F}_s$, as described in Appendix A and Fig. 1(b), causes the frame-mass-loaded SUT to move with velocity $\mathbf{v}_2(\mathrm{j}\omega)$, hence:

$$\mathbf{Y}_{\mathrm{SUT,Loaded}}(\mathrm{j}\omega) = \frac{\mathbf{v}_2(\mathrm{j}\omega)}{\mathbf{F}_s(\mathrm{j}\omega)} = \frac{-1}{\mathrm{j}\omega M_m(\mathbf{v}_1(\mathrm{j}\omega)/\mathbf{v}_2(\mathrm{j}\omega))} \tag{18}$$

Substituting Eq. (18) into Eq. (17) gives the MMD equation (Eq. (2)); this derivation shows that the loading effect of the frame mass of the device can be linearly removed resulting in the unloaded mobility.

Appendix C

C.1. Green's function

The Green's function for the mobility expression, simplified from Scherer et al. [9] for driving point mobility only, is given by

$$\begin{aligned}\mathbf{G}(\xi,\xi,\mathrm{j}\omega) = {} & \frac{1}{4\mathbf{B}^3(1+\cos[\mathbf{B}]\cosh[\boldsymbol{B}])} \\ & \times \left\{ \begin{array}{l} (\cosh[\mathbf{B}\xi]-\cos[\mathbf{B}\xi]) \\ \quad \times \left\{ \begin{array}{l} (\cosh[\mathbf{B}(\xi-1)]\sin[\mathbf{B}]+\sin[\mathbf{B}\xi]+\cosh[\mathbf{B}]\sin[\mathbf{B}(\xi-1)] \\ \quad +\cos[\mathbf{B}(\xi-1)]\sinh[\mathbf{B}]+\sinh[\mathbf{B}\xi]+\cos[\mathbf{B}]\sinh[\mathbf{B}(\xi-1)]) \end{array} \right. \\ + \\ (\sin[\mathbf{B}\xi]-\sinh[\mathbf{B}\xi]) \\ \quad \times \left\{ \begin{array}{l} (\cos[\mathbf{B}(\xi-1)]\cosh[\mathbf{B}]+\cos[\mathbf{B}\xi]+\cos[\mathbf{B}]\cosh[\mathbf{B}(\xi-1)] \\ \quad +\sin[\mathbf{B}(\xi-1)]\sinh[\mathbf{B}]+\cosh[\mathbf{B}\xi]+\sin[\mathbf{B}]\sinh[\mathbf{B}(1-\xi)]) \end{array} \right. \end{array} \right. \end{aligned} \tag{19}$$

where $\xi = x/L$ is the fractional length, and x represents the distance from the clamped end of the cantilever of the point of applied force (Fig. 3). The expression for $\mathbf{B} = \mathbf{B}(\mathrm{j}\omega)$ was simplified from Scherer's expression since for air the fluid force contribution to mobility was considered negligible for our application; hence:

$$\mathbf{B}(\mathrm{j}\omega) = \left[\frac{\mu\omega^2 L^4}{\mathbf{E}I}\right]^{1/4} \tag{20}$$

More specifically, our calculation shows that for any cantilever of width $b \leqslant 0.05\,\mathrm{m}$ in air, $\mathbf{B}(\mathrm{j}\omega)$ will not deviate from that previously described [9] by more than 0.06% for $\omega > 1\,\mathrm{rad\,s^{-1}}$.

References

[1] F.A. Firestone, A new analogy between mechanical and electrical systems, *Journal of the Acoustical Society of America* 4 (1933) 249–267.

[2] L. Beranek, *Acoustics*, McGraw-Hill, New York, 1954, pp. 51–62.

[3] G.J. O'Hara, Mechanical impedance and mobility concepts, *Journal of the Acoustical Society of America* 41 (1967) 1180–1184.

[4] International Organization for Standardization ISO 7626-1, Vibration and shock—experimental determination of mechanical mobility—part 1: basic definitions and transducers, 1986.

[5] P. Hagedorn, Some remarks on dynamic receptance, stiffness, and impedance of mechanical systems, *Journal of Applied Mathematics and Physics (ZAMP)* 37 (1986) 134–149.

[6] M.A. Sanderson, C.R. Fredö, Direct measurement of moment mobility Part I: a theoretical study, *Journal of Sound and Vibration* 179 (1995) 669–684.

[7] M.A. Sanderson, Direct measurement of moment mobility. Part II: an experimental study, *Journal of Sound and Vibration* 179 (1995) 685–696.

[8] R.S. Ming, J. Pan, M.P. Norton, The mobility functions and their application in calculating power flow in coupled cylindrical shells, *Journal of the Acoustical Society of America* 105 (1999) 1702–1713.
[9] M.P. Scherer, G. Frank, A.W. Gummer, Experimental determination of the mechanical impedance of atomic force microscopy cantilevers in fluids up to 70 kHz, *Journal of Applied Physics* 88 (2000) 2912–2920.
[10] D.J. Ewins, M.G. Sainsbury, Mobility measurements for the vibration analysis of connected structures, *The Shock and Vibration Bulletin* 42 (1972) 105–122.
[11] B. Petersson, A thin-plate model for the moment mobility at the intersection of two perpendicular plates, *Journal of Sound and Vibration* 180 (1986) 471–485.
[12] D. Otte, Coupling of structures using measured FRFs by means of SVD-based data reduction techniques, *Proceedings of the Eighth International Modal Analysis Conference*, Vol. 1, 1990, pp. 213–220.
[13] N.H. Farag, J. Pan, Dynamic response and power flow in two-dimensional coupled beam structures under in-plane loading, *Journal of the Acoustical Society of America* 99 (1996) 2930–2937.
[14] P. Gardonio, S.J. Elliot, R.J. Pinnington, Active isolation of structural vibration on a multiple-degree-of-freedom system, part I: the dynamics of the system, *Journal of Sound and Vibration* 207 (1997) 61–93.
[15] P. Gardonio, S.J. Elliot, R.J. Pinnington, Active isolation of structural vibration on a multiple-degree-of-freedom system, part II: effectiveness of active control strategies, *Journal of Sound and Vibration* 207 (1997) 95–121.
[16] S.M. Kim, M.J. Brennan, A compact matrix formulation using the impedance and mobility approach for the analysis of structural-acoustic systems, *Journal of Sound and Vibration* 223 (1999) 97–113.
[17] P. Bonello, M.J. Brennan, Modelling the dynamic behaviour of a supercritical rotor on a flexible foundation using the mechanical impedance technique, *Journal of Sound and Vibration* 239 (2001) 445–466.
[18] S.J. Elliot, L. Benassi, M.J. Brennan, P. Gardonio, X. Huang, Mobility analysis of active isolation systems, *Journal of Sound and Vibration* 271 (2004) 297–321.
[19] R.J. Pinnington, R.G. White, Power flow through machine isolators to resonant and non-resonant beams, *Journal of Sound and Vibration* 75 (1981) 179–197.
[20] J.M. Cuschieri, Excitation and response of piping systems, *Journal of the Acoustical Society of America* 83 (1988) 641–646.
[21] J.M. Cuschieri, Structural power-flow analysis using a mobility approach of an L-shaped plate, *Journal of the Acoustical Society of America* 87 (1990) 1159–1165.
[22] J.M. Cuschieri, Vibration transmission through periodic structures using a mobility power flow approach, *Journal of Sound and Vibration* 143 (1990) 65–74.
[23] B.L. Clarkson, Estimation of the coupling loss factor of structural joints, *Journal of Mechanical Engineering Science Part C* 205 (1991) 17–22.
[24] B.A.T. Petersson, Structural acoustic power transmission by point moment and force excitation, part I: beam- and frame-like structures, *Journal of Sound and Vibration* 160 (1993) 43–66.
[25] B.A.T. Petersson, Structural acoustic power transmission by point moment and force excitation, part II: plate-like structures, *Journal of Sound and Vibration* 160 (1993) 67–91.
[26] Y.K. Koh, R.G. White, Analysis and control of vibrational power transmission to machinery supporting structures subjected to a multi-excitation system, part I: driving point mobility matrix of beams and rectangular plates, *Journal of Sound and Vibration* 196 (1996) 469–493.
[27] Y.K. Koh, R.G. White, Analysis and control of vibrational power transmission to machinery supporting structures subjected to a multi-excitation system, part II: vibrational power analysis and control schemes, *Journal of Sound and Vibration* 196 (1996) 495–508.
[28] Y.K. Koh, R.G. White, Analysis and control of vibrational power transmission to machinery supporting structures subjected to a multi-excitation system, part III: vibrational power cancellation and control experiments, *Journal of Sound and Vibration* 196 (1996) 509–522.
[29] P. Gardonio, S.J. Elliot, Active control of structure-borne and air-borne sound transmission through double panels, *Journal of Aircraft* 36 (1999) 1023–1032.
[30] A.T. Moorhouse, On the characteristic power of structure-borne sound sources, *Journal of Sound and Vibration* 248 (2001) 441–459.
[31] K. Nezu, H. Kodoguchi, A new damage detection method by mechanical impedance measurements, *Bulletin of the Japan Society of Mechanical Engineers* 23 (1980) 2125–2131.
[32] M.A. Mannan, M.H. Richardson, Detection and location of structural cracks using FRF measurements, *Proceedings of the Eighth International Model Analysis Conference*, Vol. 1, 1990, pp. 652–657.
[33] G. Bamnios, A. Trochidis, Mechanical impedance of a cracked cantilever beam, *Journal of the Acoustical Society of America* 97 (1995) 3635.
[34] S. Prabhakar, A.S. Sekhar, A.R. Mohanty, Detection and monitoring of cracks using mechanical impedance of rotor-bearing system, *Journal of the Acoustical Society of America* 110 (2001) 2351–2359.
[35] S. Prabhakar, A.R. Mohanty, A.S. Sekhar, Crack detection by measurement of mechanical impedance of a rotor-bearing system, *Journal of the Acoustical Society of America* 112 (2002) 2825–2830.
[36] J.L. Edwards, D.R. Hicks, Useful range of a mechanical impedance technique for measurement of dynamic properties of materials, *Journal of the Acoustical Society of America* 52 (1972) 1053–1056.
[37] E.K. Franke, Mechanical impedance of the surface of the human body, *Journal of Applied Physiology* 3 (1951) 582–590.
[38] H. Oka, T. Yamamoto, K. Saratani, T. Kawazoe, Application of mechanical mobility of periodontal tissues to tooth mobility examination, *Medical and Biological Engineering and Computing* 27 (1989) 75–81.

[39] J.Z. Wu, R.G. Dong, D.E. Welcome, Analysis of the point mechanical impedance of fingerpad in vibration, *Medical Engineering and Physics* 28 (2006) 816–826.
[40] A.Z. Hajian, R.D. Howe, Identification of the mechanical impedance at the human finger tip, *Journal of Biomechanical Engineering* 119 (1997) 109–114.
[41] P. Holmlund, R. Lundström, Mechanical impedance of the human body in the horizontal direction, *Journal of Sound and Vibration* 215 (1998) 801–812.
[42] R.E. Kearney, I.W. Hunter, System identification of human joint dynamics, *Critical Reviews in Biomedical Engineering* 18 (1990) 55–87.
[43] E. Burdet, R. Osu, D.W. Franklin, T.E. Milner, M. Kawato, The central nervous system stabilizes unstable dynamics by learning optimal impedance, *Nature* 414 (2001) 446–449.
[44] M. Darainy, F. Towhidkhah, D.J. Ostry, Control of hand impedance under static conditions and during reaching movement, *Journal of Neurophysiology* 97 (2007) 2676–2685.
[45] M.P. Scherer, A.W. Gummer, Impedance analysis of the organ of corti with magnetically actuated probes, *Biophysical Journal* 87 (2004) 1378–1391.
[46] M. Massoud, H. Pastorel, Impedance methods for machine analysis, *The Shock and Vibration Digest* 10 (1978) 9–18.
[47] International Organization for Standardization ISO 7626-5, Vibration and shock—experimental determination of mechanical mobility—part 5: measurements using impact excitation with an exciter which is not attached to the structure, 1994.
[48] C.D. Van Karsen, E.F. Little, The strengths of impact testing, *Proceedings of the 15th IAMC*, Orlando, FL, 1997, pp. 1667–1671.
[49] D. Brown, Weaknesses of impact testing, *Proceedings of the 15th IAMC*, Orlando, FL, 1997, pp. 1672–1676.
[50] International Organization for Standardization ISO 7626-2, Vibration and shock—experimental determination of mechanical mobility—part 2: measurements using single-point translation excitation with an attached vibration exciter, 1990.
[51] M.H. Wilkinson, Measuring Tissue Mobility, US Patent No. US 7201721 B2, 2007.
[52] M.H. Wilkinson, Measuring Tissue Mobility, UK Patent No. GB 2404989 A, 2005.
[53] R.D. Blevins, *Formulas for Natural Frequency and Mode Shape*, Van Nostrand Reinhold, New York, 1979, pp. 43.
[54] L.E. Kinsler, A.R. Frey, *Fundamentals of Acoustics*, second ed., Wiley Inc., New York, 1962, pp. 75.
[55] J.E. Sader, Frequency response of cantilever beams immersed in viscous fluids with applications to the atomic force microscope, *Journal of Applied Physics* 84 (1998) 64–76.